Recharging autonomous underwater vehicles from ambient wave induced motions

Nicholas Townsend and Ajit Shenoi.

***Abstract*—In this paper a novel gyroscopic system capable of recharging an autonomous underwater vehicle (AUV) using wave energy is proposed. The system, which is based on control moment gyroscope (CMG) principles, utilises the gyroscopic response of a gimballed flywheel mounted within an AUV body to generate energy from the wave induced rotational motions of the vehicle. By utilising the wave induced rotational motions of an AUV and the relative motion/torque created by a precessing gimballed flywheel promises to enable AUVs to generate energy *in-situ* and from a renewable source. This novel approach has several advantages. As the system is housed internally it is not exposed to the harsh underwater environment, is not susceptible to bio-fouling and does not add any hydrodynamic drag. In addition, the system can be positioned anywhere within the AUV body and the technology has the potential to be developed into an integrated energy harvesting, storage and motion control system; whereby the wave induced gyroscopic precession of the flywheel can be used to generate energy, the flywheel kinetic energy (spin) can be utilised for energy storage (similar to Kinetic Energy Recovery Systems or KERS) and motion control can be provided by precession control of the flywheel (providing a stable platform for improved monitoring/recording capabilities).**

In this paper a theoretical description of the system is provided including a derivation of the governing equations of motion following a momentum (Newton-Euler) approach. A numerical model is also described and simulation results for a pitching 2m AUV system are presented. The results show that the system could be used to periodically recharge an AUV remotely, enabling longer AUV deployments at sea.

***Index Terms*—Autonomous Underwater Vehicles (AUVs), gyroscopic systems, renewable energy, wave energy.**

I. Introduction

Nearly all autonomous underwater vehicles (AUVs) depend on stored energy for their operation [1]. To increase AUV endurance which is typically measured in hours or days [1], *in-situ* battery charging and/or alternative power systems are required. The majority of Autonomous Underwater Vehicles (AUVs) use batteries as an energy supply for their operation [2, 3]. However, batteries are limited. They require periodical recharging (and redeployment) from a dedicated host platform or support vessel and represent a significant proportion of the total vehicle mass, typically around 20% [1]. In addition, with many of the high performance batteries prohibitively expensive for AUV applications [2], alternative power sources or *in-situ* recharging are needed.

In the past, internal combustion engines have been used to power AUVs. However, these systems are limited as additional power is needed to expel the exhaust gases at depths greater than 200m [3]. The Royal Swedish Navy has used Stirling engines [3] and (Slocum) gliders have been developed using ocean temperature gradients and battery power to generate propulsion [4]. Fuel cells have been trialled on the AUV URASHIMA [5] and solar powered AUVs, the SAUV-I and SAUV-II, have also been developed [6]. Although the SAUV II potentially offers unlimited mission durations, it is limited to night-time missions and daylight recharging strategies [6]. Furthermore, the SAUV II is susceptible to bio fouling [6]. Ideas of recharging AUV power supplies using wave-energy absorbers and sea current generators have also been proposed [7], [8] however, no practical demonstrations have been made.

In this paper a novel gyroscopic system capable of recharging an AUV using wave energy is proposed and performance predictions for a 2m AUV system are presented. The system, illustrated in Fig.1 and Fig.2, uses the wave induced gyroscopic precession of a flywheel mounted within an AUV's body to generate power. Although combined energy storage and attitude control of underwater robots (AUVs) using gyrostabiliser technology has been demonstrated [9], [10] and gyroscopic wave energy converters are under development in Japan [11]–[13], Italy [14]–[16] and Spain [17]. To the author's knowledge, this is the first study to consider gyroscopic wave energy harvesting as a means of renewably and remotely recharging an AUV, where the power constraints can severely limit performance.

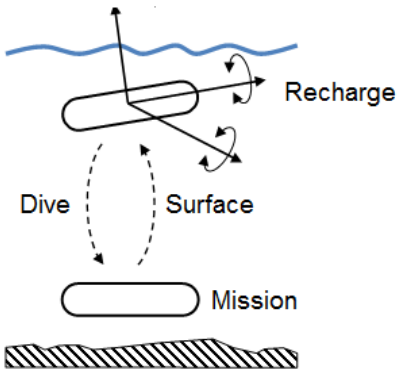

Fig. 1. Operational schematic

As the effect of surface waves and swell diminishes with depth [18], similar to SAUV II, the AUV system would

need to surface to recharge, as depicted in Fig.1. However, the system would not be limited to daylight recharging and night time missions. In addition, as waves are a concentrated form of solar energy (formed by winds passing over bodies of water created by the differential heating of air masses by the sun on the earth's atmosphere) greater energy capture is anticipated, compared to solar strategies. Furthermore, with no direct exposure to the marine environment the system would not be susceptible to environmental performance degradations i.e., bio fouling. However, the AUV would be exposed to the potentially hazardous wave environment. In conjunction with the low locational dependency, the kinetic energy storage capabilities (utilising the flywheel spin) and motion control (by controlling the precession rate) the system has the potential to improve AUV performance, reducing AUV battery requirements and indefinitely extending missions.

The paper outline is as follows; In Section 2 a theoretical description of the system is presented including a derivation of the governing equations of motion following a momentum (Newton-Euler) approach. In Section 3 the numerical model and simulation parameters are presented. The results of the numerical model are presented in Section 4 and a discussion of the results follows in Section 5.

II. Theory

A. Coordinate Systems

To describe the system four right handed coordinate frames were used, as shown in Fig.2.

- (X_e, Y_e, Z_e) represents an Earth fixed inertial axis system.
- (X_h, Y_h, Z_h) represents the hydrodynamic or equilibrium axis system that moves with the average motion of the AUV but is not fixed to the AUV.
- (X_b, Y_b, Z_b) represents the body (AUV) fixed axis system.
- (X_f, Y_f, Z_f) represents the flywheel axis system. This axis precesses but does not spin with the flywheel.

As shown in Fig.2, the coordinate frames were assumed to have corresponding centres and the body and flywheel frames of reference to coincide with the principal axes of inertia of the AUV and flywheel. In this study, the flywheel restricted, spin and precessional axis angles are denoted by (ϵ, ψ, β) respectively and represent the flywheel rotations from (X_f, Y_f, Z_f) into (X_b, Y_b, Z_b). The rotations about the AUV body fixed axis system (X_b, Y_b, Z_b) are denoted by (θ, ϕ, γ) and represent the rotations from (X_b, Y_b, Z_b) to (X_h, Y_h, Z_h).

B. Gyroscopic Motion

1) Gyroscopic moments about the body fixed axis: Following a momentum (Newton-Euler) method and neglecting the gimbal components and initially the AUV motion effects (identified by subscript $b*$), the angular momentum in the AUV body fixed axis system (X_b, Y_b, Z_b) can be expressed as;

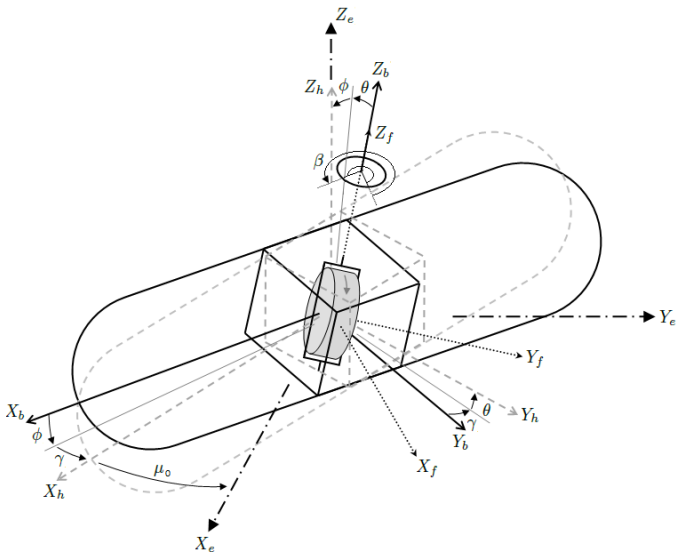

Fig. 2. System schematic and coordinate frame definitions

$$\underline{H}_{b*} = \underline{A}_f^b \, \underline{H}_f = \underline{A}_f^b \underline{I}_f \underline{\omega}_f$$

where $\underline{\omega}_f$ and $\underline{I}_f$ represent the angular motions and mass moment of inertia of the flywheel, with respect to (X_f, Y_f, Z_f). $\underline{H}_f$ and $\underline{H}_b$, 3×1 column vectors, represent the angular momentum of the flywheel about the flywheel and body fixed axis respectively. $\underline{A}_f^b$ represents the rotation matrix describing the transformation of the momentum component expressed in the AUV body fixed axis when the component is rotated from (X_f, X_f, X_f) to (X_b, X_b, X_b).

Including the AUV motion effects, the moments acting around each axis in the AUV body-fixed coordinate frame (X_b, Y_b, Z_b) can be expressed as;

$$\dot{\underline{H}}_b = \dot{\underline{H}}_{b*} + \underline{\Omega}^{\times} \underline{H}_{b*} = \frac{d}{dt}(\underline{A}_f^b \, \underline{I}_f \, \underline{\omega}_f) + \underline{\Omega}^{\times} \, \underline{A}_f^b \, \underline{I}_f \, \underline{\omega}_f \quad (1)$$

Here $\underline{H}_{b*}$ represents the relative angular momentum and $\underline{\Omega}^{\times}$ represents the skew-symmetric form (equivalent to the cross product operation) of the body motions experienced by the flywheel, that is;

$$\underline{\Omega}^{\times} = \begin{bmatrix} 0 & -\dot{\gamma} & \dot{\phi} \\ \dot{\gamma} & 0 & -\dot{\theta} \\ -\dot{\phi} & \dot{\theta} & 0 \end{bmatrix} \quad (2)$$

By the product rule $(\frac{d}{dt}(uv) = udv + vdu)$ and as $(v^T du^T)^T = vdu$;

$$\frac{d}{dt}(\underline{A}_f^b \, \underline{I}_f \, \underline{\omega}_f) = \underline{A}_f^b \, \underline{I}_f \, \dot{\underline{\omega}}_f + (\underline{\omega}_f^T \, (\dot{\underline{A}}_f^b \, \underline{I}_f)^T)^T \quad (3)$$

Using the transpose of a product $(AB)^T = B^T A^T$, the

gyroscopic moments about the body fixed axis can then be expressed as;

$$\begin{aligned}\dot{\underline{H}}_b &= \underline{A}^b_f\,\underline{I}_f\,\dot{\underline{\omega}}_f + (\underline{\omega}^T_f\,(\dot{\underline{A}}^b_f\,\underline{I}_f)^T)^T + \underline{\Omega}^{\times}\,\underline{A}^b_f\,\underline{I}_f\,\underline{\omega}_f \\ &= (\underline{A}^b_f\,\underline{I}_f)\dot{\underline{\omega}}_f + (\dot{\underline{A}}^b_f\,\underline{I}_f + \underline{\Omega}^{\times}\,\underline{A}^b_f\,\underline{I}_f)\underline{\omega}_f \end{aligned} \quad (4)$$

For the one flywheel system considered in this study, as illustrated in Fig.2, assuming the flywheel is restricted about the x-axis (X_f), precesses about the z-axis (Z_f) and has an angular velocity, $\dot{\psi}$, about the y-axis (Y_f) and the flywheel and AUV centres of mass lie at the origin of the body-frames of reference and the body-frames of reference coincide with the principal axes of inertia of the bodies, then;

$$\underline{A}^b_f = \begin{bmatrix} cos\beta & sin\beta & 0 \\ -sin\beta & cos\beta & 0 \\ 0 & 0 & 1 \end{bmatrix} \quad (5)$$

$$\underline{I}_f = \begin{bmatrix} I_{xx} & 0 & 0 \\ 0 & I_{yy} & 0 \\ 0 & 0 & I_{zz} \end{bmatrix} \quad (6)$$

$$\underline{\omega}_f = [0\ \dot{\psi}\ \dot{\beta}]^T \quad (7)$$

where the rotation matrix has been expressed using Euler angles. Expanding Equation 4 the gyroscopic moments can then be fully expressed as;

$$\dot{\underline{H}}_b = \begin{bmatrix} I_{yy}\ddot{\psi}sin\beta + I_{yy}\dot{\psi}\dot{\beta}cos\beta - I_{yy}\dot{\psi}\dot{\gamma}cos\beta + I_{zz}\dot{\phi}\dot{\beta} \\ I_{yy}\ddot{\psi}cos\beta - I_{yy}\dot{\psi}\dot{\beta}sin\beta + I_{yy}\dot{\psi}\dot{\gamma}sin\beta - I_{zz}\dot{\theta}\dot{\beta} \\ I_{zz}\ddot{\beta} - I_{yy}\dot{\psi}\dot{\phi}sin\beta + I_{yy}\dot{\psi}\dot{\theta}cos\beta \end{bmatrix} \quad (8)$$

2) Available Power: Modelling the power take-off as a linear damper, the equation of motion about the flywheel precession axis (Z_f) can be expressed as;

$$I_{zz}\ddot{\beta} - I_{yy}\dot{\psi}\dot{\phi}sin\beta + I_{yy}\dot{\psi}\dot{\theta}cos\beta = I_g\ddot{\beta} + B_g\dot{\beta} + C_g\beta \quad (9)$$

where I_g and C_g represent the inertial and restoring terms accounting for the power take off mechanism and B_g represents the damping term accounting for the precession power take off. The instantaneous power absorbed by the damper (due to the flywheel precession) can then be expressed as;

$$P(t) = B_g\dot{\beta}^2 \quad (10)$$

III. Method

To identify the performance of the system a numerical model was developed and implemented in MATLAB [19] as outlined in Fig.3.

The modelled AUV, a cylindrical AUV with hemispherical nose and tail sections, was approximately based on a scaled Autosub6000 AUV e.g., the DELPHIN2 AUV [20]–[22] (see Fig.4 and Table I) and assumed to be fully submerged,

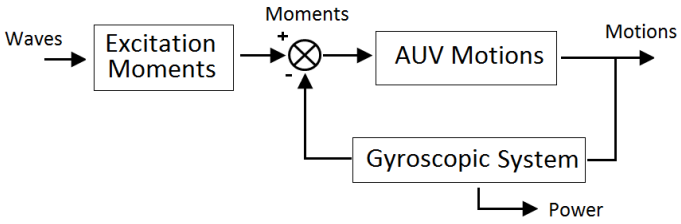

Fig. 3. Block diagram representation of the system

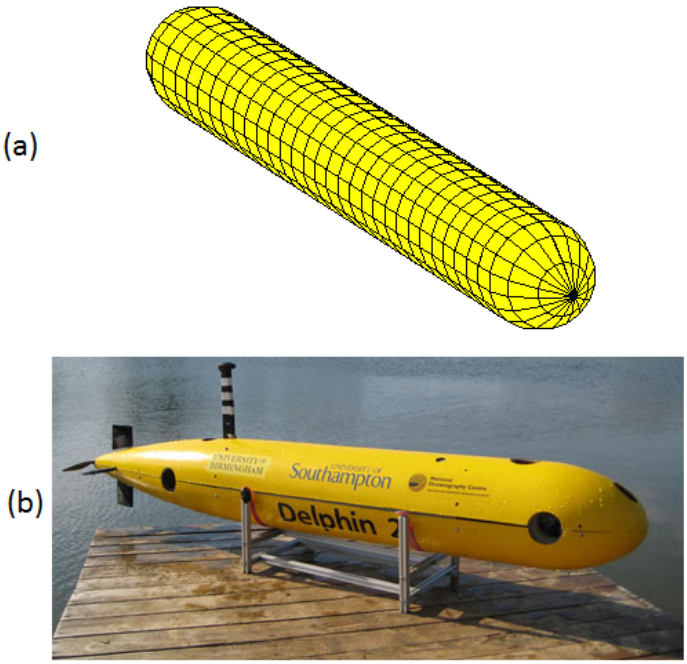

Fig. 4. (a) The simplified AUV model (b) the DELPHIN2 AUV

just below the surface. The AUV motions were modelled in 1 degree of freedom (pitch) with a (pseudo-time) time domain, linear seakeeping model. In this study a pitch model was considered because the excitation moments are typically greater in pitch than roll and it readily allows for experimental validation in a (small) towing tank. Coupling the AUV and gyroscopic motions the equation of motion can be expressed as;

$$\begin{aligned}(I_{55} + A_{55}(\omega))\ddot{\phi} + B_{55}(\omega)\dot{\phi}(\omega) + C_{55}\phi \\ = F_5(\omega)cos(\omega t + \Phi_5) - (\dot{H}_b)_y \end{aligned} \quad (11)$$

assuming small AUV angles (such that the body fixed gyroscopic terms and hydrodynamic axis frame excitation moments can be equated). Here $A_{55}(\omega)$ and $B_{55}(\omega)$ represent the frequency dependent pitch added mass and damping coefficients, respectively. $\Phi_5(\omega)$ and $F_5(\omega)$ represent the phase and amplitude of the pitch wave excitation moment. Equation 11 provides a means to readily explore system parameters and is widely used within wave energy converter literature to assess system performance. However, it should

be noted that Equation 11 (omitting the gyroscopic terms) describes the AUV motions in steady state and is only valid for discrete frequencies, where the frequency dependent fixed coefficients take their respective frequency dependent value. That is, Equation 11 does not account for the fluid memory effects and does not allow for arbitrary excitation, i.e., irregular waves.

The regular wave excitation moment amplitudes ($F_5(\omega)$), phases ($\Phi_5(\omega)$) and the frequency dependent added mass ($A_{55}(\omega)$) and damping ($B_{55}(\omega)$) coefficients, were identified over a range of frequencies using a hydrodynamic panel code (in this study the linear potential flow, three dimensional ship motion programme THARBM [23] was used). The results are presented in Fig.5 and Fig.6.

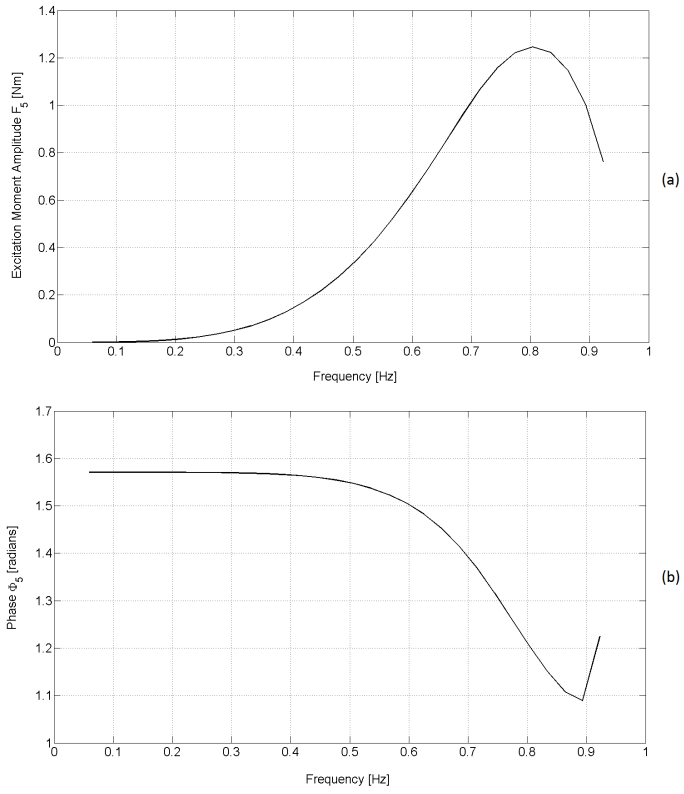

Fig. 5. Pitch excitation moments F_5 (a) and phases Φ_5 (b) (wave amplitude of 0.1m)

To solve the equations of motion, initially the gyroscopic moments about the body axis (Equation 4) were determined from the initialised motions. Interpolating from Fig.5(a) and Fig.5(b), the wave excitation and phases were determined (for a given wave frequency and amplitude) and used to generate a time history of the wave excitation moments. Then, based on the fourth-order Runge-Kutta integration scheme, Equations 11 and 9 were solved for the body and gyroscopic precession motions respectively, assuming a constant flywheel angular velocity. The power was then calculated using Equation

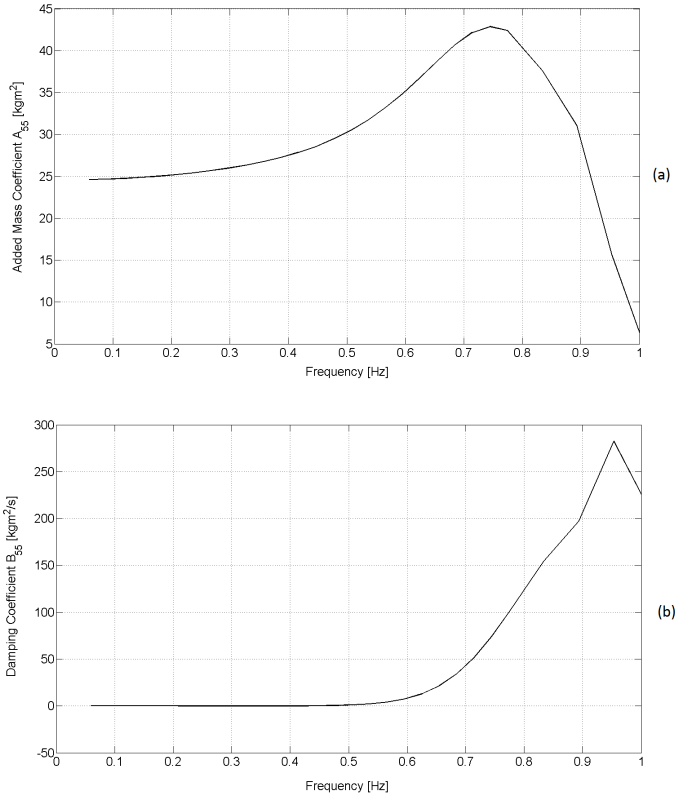

Fig. 6. Hydrodynamic coefficients ((a) Added mass A_{55} (b) Damping B_{55})

10. By repeating this procedure at every time step, a time history of the motion responses and available power was generated, for the given conditions. The simulation parameters are summarised in Table I and the results follow in Section IV.

TABLE I
SIMULATION SUMMARY

AUV particulars	**Value**
Overall length $[m]$	2
Diameter $[m]$	0.243
Displacement $[kg(m^3)]$	83.9650 (0.0819)
Pitch restoring coefficient $(C_{55})[Nm]$	9.4137
Vertical centre of gravity (from AUV top, down) $[m]$	0.133
$\overline{BG}[m]$	0.0115
Longitudinal centre of gravity (from FP) $[m]$	1
Mass moment of inertia $(I_{55})[kgm^2]$	15.8106
Gyroscopic system particulars	**Value**
Flywheel mass moment of inertia $(I_{yy})[kgm^2]$	0.004
Flywheel mass moment of inertia $(I_{xx} = I_{zz})[kgm^2]$	0.0034
e.g. Flywheel mass $[kg]$	1.68 ($\approx 2\%$ mass)
e.g. Flywheel diameter $[m]$	0.08
Flywheel spin rate $[rpm]$ (assumed constant)	5000 to 40000
PTO inertia coefficient $(I_g)[Nm.s^2]$	0.0034
PTO damping coefficient $(B_g)[Nm.s]$	0.1 to 10
PTO restoring coefficient $(C_g)[Nm]$	5 sin($\beta_{i-1} - \pi/2$)
Simulation parameters	**Value**
Time step $[s]$	0.05
Simulated time $[s]$	200
Numerical integration scheme	ODE45
Absolute and relative error tolerance	1e-10
Linear ramp length $[s]$	40
Heading (fixed, head waves) $[radians]$	π
Excitation frequencies (wave frequencies) $[rad/s]$	0.88 to 5.7
Wave Amplitude $[m]$	0.1

A. Simulation Parameters

A summary of the modelled AUV and gyroscopic system particulars are presented in Table I. The simulations were made assuming the flywheel to have a constant angular velocity (spin rate) and the precession motion started from rest. That is, $\ddot{\psi} = 0\ rad/s^2$ and $\beta = \pi/2\ rad$, $\dot{\beta} = 0\ rad/s$. The wave excitation was also linearly ramped up to minimise the initial transient motions.

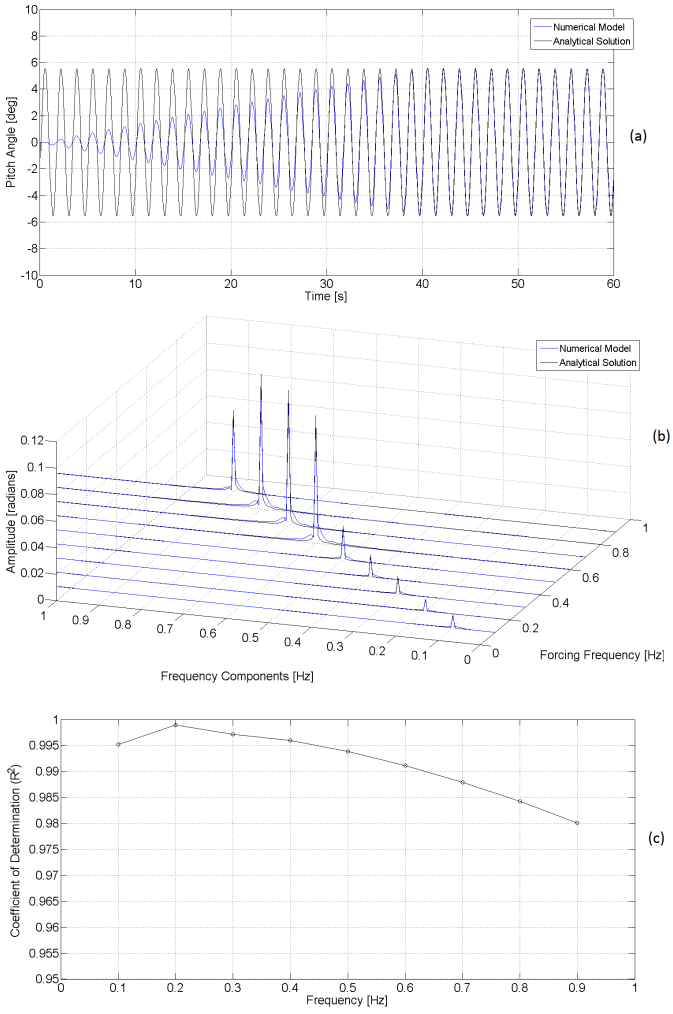

Fig. 7. Comparison of numerical and analytical solutions ((a): Example time history (frequency= 0.6Hz) (b): Frequency responses (c): Coefficient of determination (R^2))(dt=0.05)

B. Verification

1) Analytical Comparison: Ignoring the gyroscopic system (i.e., $\dot{\psi} = 0$, $\dot{\beta} = 0$) the equation of motion (Equation 11) simplifies to a 2nd order linear nonhomogeneous constant-coefficient differential equations. That is;

$$(I_{55} + A_{55}(\omega))\ddot{\phi} + B_{55}(\omega)\dot{\phi} + C_{55}\phi = F_5 cos(\omega t) \quad (12)$$

The particular solution, or steady state response of the system can then be expressed as;

$$\phi(t) = [A_p cos(\omega t) + B_p sin(\omega t)] \quad (13)$$

where A_p and B_p can be found by differentiating and substituting Equation 13 into Equation 12 and equating coefficients of $cos(\omega t)$ and $sin(\omega t)$.

A comparison of this analytical approach and the numerical method is given in Fig.7. The numerical model assumed the system started from rest ($\phi, \dot{\phi}, \ddot{\phi} = 0$) and the wave excitation was linearly ramped up. This was made in an attempt to minimise the initial transient motions. The effect of the ramp function is presented in Fig.7(a). The coefficient of determination (R^2), representing the difference between the analytical and numerical solutions over a range of frequencies are presented in Fig.7(c). The differences between the analytical and numerical steady state results were found to be negligible, providing confidence in the numerical solutions.

2) Numerical Method Parameters: The effect of solving the equation of motion (Equation 11) using varying time steps, integration solver and error tolerance is given in Fig.8. As shown in Fig.8(a) with small, periodic responses of the gyroscope a convergence of the results is observed with smaller time steps. The results were also found to be robust, with no significant differences when varying the allowed error tolerances or the integration scheme, see Fig.8(b) and (c). These findings, in addition to the close agreement with the analytical solution, provide confidence in the numerical method and solutions. However, interestingly for nonlinear responses of the gyroscope the solution was observed to become extremely sensitive. That is, any slight changes (whether time step, error tolerance and/or numerical integration) caused the results to deviate substantially over time, as illustrated in Fig.8(d). Although the response characteristics remain similar these deviations, a general feature of nonlinear models, make it difficult to verify the nonlinear responses. In order for the nonlinear cases to be identified with some confidence, the simulation parameters, see Table I, were selected conservatively.

IV. Results

The results of the numerical model presented in this paper are based on 0.1m wave amplitude regular waves, in preparation for experimental validation tests. A range of excitation (wave) frequencies between 0.88 to 5.7 rad/s were modelled and the system parameters of spin rate ($\dot{\psi}$) and power take off damping coefficient (B_g) were investigated.

The effect of spin rate on the gyroscopic response is illustrated in Fig.9 and the available rms power is presented in Fig.11, for a range of forcing frequencies, damping coefficients (B_g) and spin rates. Example gyroscopic

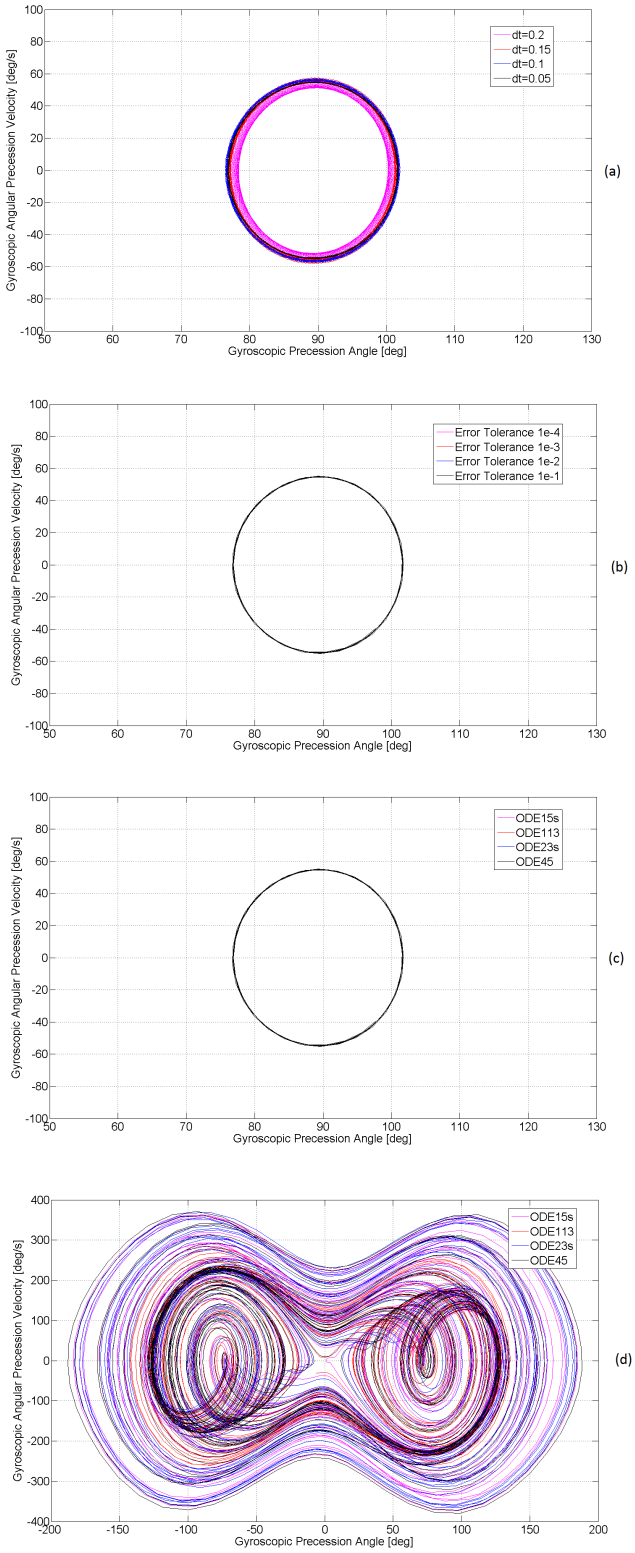

Fig. 8. Numerical method verification ((a): Effect of time step (b): Effect of numerical integration scheme (c): Effect of error tolerance (d): Nonlinear response) ((a)-(c) 10,000rpm (d) 30,000rpm)(ω = 0.7Hz, ODE45, Error Tolerance: $1e-10$, dt=0.05, unless otherwise stated.)

responses and instantaneous powers are presented in Fig.10 and Fig.12, in both time and frequency domains.

Fig.9 shows the gyroscopic response of the system with various spin rates to a regular wave excitation (ω= 4.76 rad/s), with a fixed damping coefficient (B_g=0.3 $Nm.s$). Initially, with an increase in spin rate the gyroscopic response was found to increase, with a frequency equal to the forcing frequency. However, with further increases in spin rate the gyroscopic response was found to become nonlinear, exhibiting multiple frequency components. As shown in Fig.9(a), with lower spin rates the gyroscopic precession behaves linearly oscillating within the region 0^o to 180^o, about 90^o due to the restoring term (C_g). With further increases in spin rate the gyroscopic response can exceed the region 0^o to 180^o, oscillating with multiple frequency components.

An example of the linear and nonlinear responses are presented in Fig.10. The linear responses exhibit gyroscopic oscillations about 90^o within the region 0^o and 180^o, with a frequency equal to the forcing frequency. Typically the linear gyroscopic responses occur with low, non-resonance excitation moments and a high power take off damping coefficient (B_g). With an increase in the excitation moments, for example around resonance, and lower damping characteristics (B_g) the gyroscopic responses increase and can exhibit nonlinear responses. As shown in Fig.10 these are often characterised by irregular, multiple frequency component responses. Interestingly, provided non-linear motions are allowed to develop, greater precession rates and instantaneous powers are available. As expected, Fig.10 shows that the power typically has a frequency of twice the principal gyroscopic response.

The available rms power over a range of frequencies, damping coefficients and spin rates is given in Fig.11, for the modelled system. At low spin rates (small angular momentum) very little power is available. However, with increasing spin rates and around resonance the system can generate useful amounts of power, in what are relatively small waves (0.1m amplitude). Interestingly, the model also predicts high power at low wave excitation frequencies and small damping coefficients. The validity of this needs to be confirmed experimentally.

V. Discussion

The numerical model results show that with the appropriate system parameters ($\dot{\psi}$ and B_g) and excitation frequency (ω) the system can generate power, with the maximum power available around resonance. Interestingly, the model also predicts high power at low wave excitation frequencies and small damping coefficients (B_g). In theory continually reducing the damping characteristic (B_g), could enable high gyroscopic precession rates and power to be generated, as the

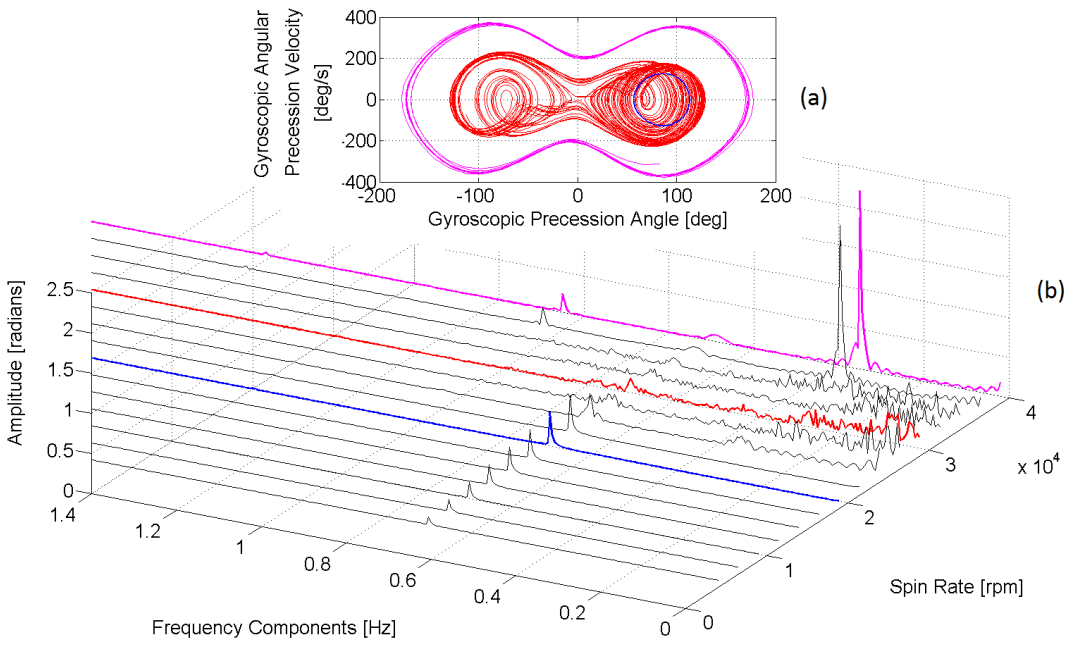

Fig. 9. Gyroscopic precession responses over a range of spin rates ((a) Example phase plots (magenta:40000rpm, red:30000rpm, blue:20000rpm)(b) Frequency response over a range of spin rates)(ω=0.7Hz,B_g=0.3)

system would become very sensitive responding nonlinearly to relatively small excitations. However, given that the model does not account for frictional loses in the system, assumes small AUV angles and only considers AUV motion in 1 degree of freedom, it is anticipated that the low frequency nonlinear responses are unrealistic.

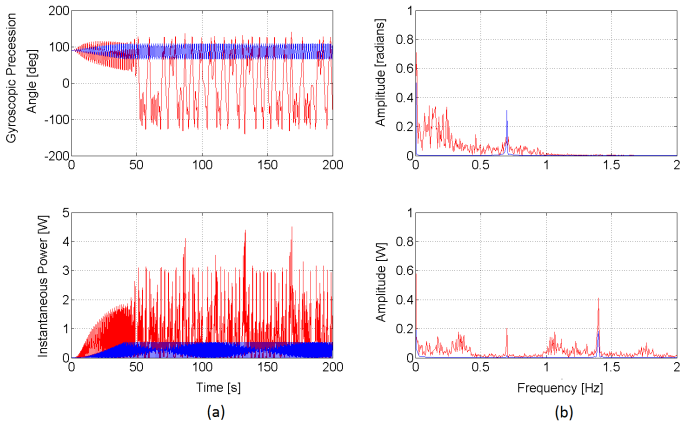

Fig. 10. Example gyroscopic precession and instantaneous power for a linear (blue, 15000rpm) and nonlinear (red, 30000rpm) response ((a) Time domain response (b) Frequency domain response)($\omega = 0.7$Hz, B_g=0.2)

The numerical model results also identified that the system can exhibit linear and nonlinear responses, similar to the findings reported in [24]–[26]. Provided non-linear motions are allowed to develop, greater precession rates and instantaneous powers are available. Potentially, the nonlinear responses may enable greater power to be generated, however, the available power would be irregular and in practice would require an effective conversion and storage solution to efficiently capture the wide bandwidth.

Given that comparable AUVs of similar displacement have a hotel load of around 10-30W [27]. The 5-10W recharge potential predicted suggests the proposed system, albeit maybe requiring the introduction of power management and/or recharging strategies, should enable AUVs to operate for indefinite periods of time. By way of example, the Delphin2 AUV (a relative energy hungry system) has a custom built 30 Ah, 21.6 V (nominal), 10kg, Nickel Metal Hydride (NiMH) (70Wh/kg) battery pack, providing approximately 8 hours of use [22]. Assuming continuous operation for 8 hours and the batteries providing 3.75A continuously (30Ah), a power output of 81W or specific power of 8.1W/kg is required to operate the AUV. In comparison, based on the predicted 5-10W recharge potential, assuming the total gyroscopic system is $\approx 3kg$, the system has a specific power of 1.67-3.33 W/kg. Alternatively stated that is 8 to 16 times the operation time is required for complete recharge, for the assumed system and conditions.

VI. Conclusions

This paper described a novel gyroscopic system capable of recharging an autonomous underwater vehicle (AUV) using wave energy. A theoretical description of the system was provided including a derivation of the governing equations of

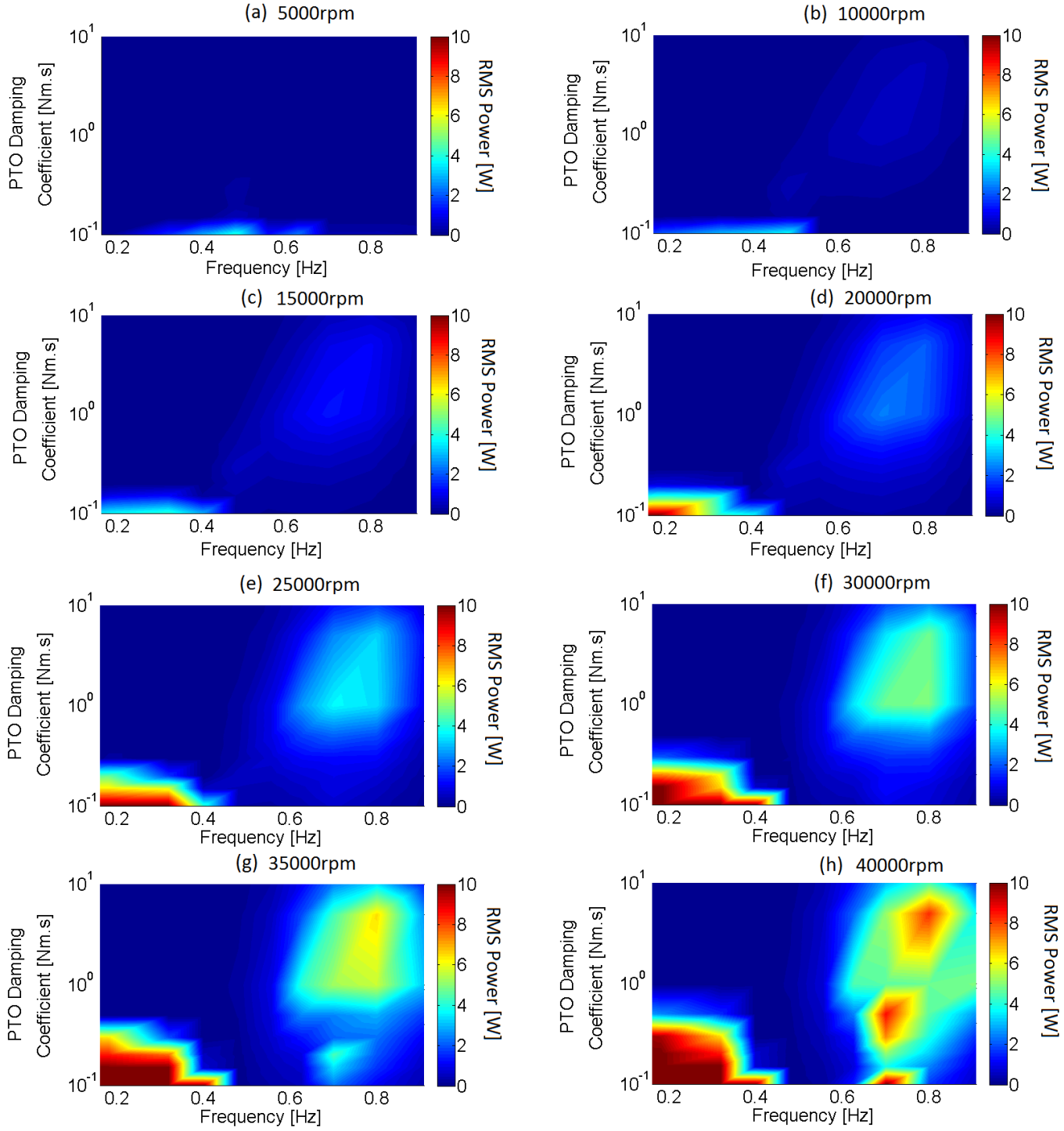

Fig. 11. Available rms power for the modelled 2m, 84kg cylindrical AUV in 0.1m wave amplitudes

motion following a momentum (Newton-Euler) approach and a numerical model was developed. Simulation results for a pitching 2m AUV system were presented. The results showed that the system could be used to periodically recharge an AUV remotely, enabling longer AUV deployments at sea.

Interestingly, linear and nonlinear gyroscopic responses were identified. Typically linear gyroscopic responses occur with low, non-resonance excitation moments and a high power take off damping coefficient (B_g). With an increase in the excitation moments, for example around resonance, and lower damping characteristics (B_g) the gyroscopic responses

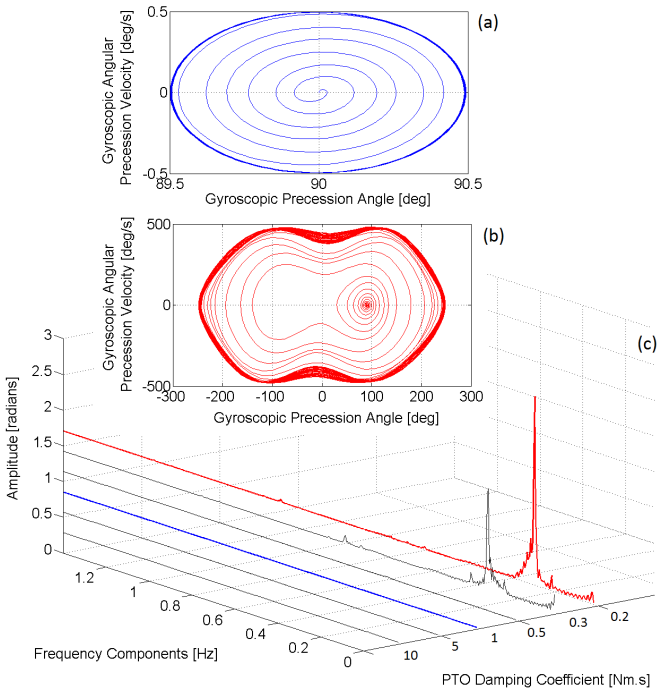

Fig. 12. Example low frequency gyroscopic precession responses ((a) Linear response (blue, B_g=1Nm.s) (b) Predicted nonlinear response (red, B_g=0.2Nm.s) (c) Frequency response over a range of damping coefficients (B_g))(ω=0.16Hz, 35000rpm)

increased and were found to exhibit nonlinear responses and instantaneously high powers.

This novel approach to recharge autonomous underwater vehicles *in-situ*, from the ambient wave induced motions has several advantages. As the system is housed internally it is not exposed to the harsh underwater environment, is not susceptible to bio-fouling and does not add any hydrodynamic drag. In addition, the system can be positioned anywhere within the AUV body and the technology has the potential to be developed into an integrated energy harvesting, storage and motion control system; whereby the wave induced gyroscopic precession of the flywheel can be used to generate energy, the flywheel kinetic energy (spin) can be utilised for energy storage (similar to Kinetic Energy Recovery Systems or KERS) and motion control can be provided by precession control of the flywheel (providing a stable platform for improved monitoring/recording capabilities). Further research is required but based on the initial results presented, the technology looks promising.

ACKNOWLEDGMENT

This research was supported by the Lloyd's Register Foundation.

REFERENCES

[1] G. Griffiths, J. Jamieson, S. Mitchell, and K. Rutherford, "Energy storage for long endurance AUVs," *Proceedings of Advances in Technology for Underwater Vehicles, London, UK*, pp. 8–16, 2004.

[2] G. Griffiths, D. Reece, P. Blackmore, M. Lain, S. Mitchell, and J. Jamieson, "Modeling hybrid energy systems for use in AUVs," *Proc. 14th Unmanned Untethered Submersible Technology (UUST)*, 2005.

[3] G. Reader, J. Potter, and J. Hawley, "The evolution of AUV power systems," *OCEANS '02 MTS/IEEE*, vol. 1, pp. 191–198, 2002.

[4] R. Davis, C. Eriksen, and P. Jones, "Autonomous buoyancy-driven underwater gliders," *The Technology and Applications of Autonomous Underwater Vehicles*, pp. 37–58, 2002.

[5] T. Hyakudome, T. Aoki, T. Murashima, S. Tsukioka, H. Yoshida, H. Nakajoh, T. Ida, S. Ishibashi, and R. Sasamoto, "Key technologies for AUV 'URASHIMA'," *OCEANS '02 MTS/IEEE*, vol. 1, pp. 162–166, 2002.

[6] D. Crimmins, C. Patty, M. Beliard, J. Baker, J. Jalbert, R. Komerska, S. Chappell, and D. Blidberg, "Long-endurance test results of the solar-powered AUV system," *OCEANS '06*, pp. 1–5, 2006.

[7] G. Hagerman, "Wave energy systems for recharging AUV energy supplies," *Proceedings of the Symposium on Autonomous Underwater Vehicle Technology*, pp. 75–84, 2002.

[8] R. Camilli, A. Bowen, and N. Farr, "Bright Blue: Advanced technologies for marine environmental monitoring and offshore energy," *OCEANS '10*, 2010.

[9] B. Thornton, T. Ura, Y. Nose, and S. Turnock, "Zero-G class underwater robots: Unrestricted attitude control using control moment gyros," *IEEE Journal of Oceanic Engineering*, vol. 32(3), 2007.

[10] B. Thornton, T. Ura, and Y. Nose, "Combined energy storage and three-axis attitude control of a gyroscopically actuated AUV," *OCEANS '08*, 2008.

[11] H. Kanki, S. Arii, T. Furusawa, and T. Otoyo, "Development of advanced wave power generation system by applying gyroscopic moment," *Proceedings of the 8th European Wave and Tidal Energy Conference (EWTEC), Uppsala, Sweden*, pp. 280–283, 2009.

[12] H. Kanki, "Gyro wave activated power generator and a wave suppressor using the power generation, patent US 7,003,947 B2," 2006.

[13] H. Kanki, T. Morimoto, M. Kawanishi, T. Onishi, and T. Hata, "Study on dynamics of floating wave-power generating system using gyro moment," *The Japan Society of Mechanical Engineers*, vol. 80, pp. 6.57–6.58, 2005.

[14] G. Bracco, E. Giorcelli, G. Mattiazzo, M. Pastorelli, and J. Taylor, "ISWEC: design of a prototype model with gyroscope," *International Conference on Clean Electrical Power*, pp. 57–63, 2009.

[15] G. Bracco, E. Giorcelli, F. Marignetti, and G. Mattiazzo, "ISWEC: Application of linear tubular generators," *IEEE International Symposium on Industrial Electronics*, pp. 2426–2430, 2010.

[16] G. Bracco, E. Giorcelli, and G. Mattiazzo, "ISWEC: A gyroscopic mechanism for wave power exploitation," *Mechanism and Machine Theory*, vol. 46, no. 10, pp. 1411 – 1424, 2011.

[17] F. Salcedo, P. Ruiz-Minguela, R. Rodriguez, P. Ricci1, and M. Santos, "OCEANTEC: Sea trials of a quarter scale prototype," *Proceedings of 8th European Wave Tidal Energy Conference (EWTEC), Uppsala, Sweden*, p. 460465, 2009.

[18] E. Levine, L. Goodman, and C. Lubke, "AUV-based swell characterization," *IEEE/OES Autonomous Underwater Vehicles*, pp. 1–6, 2008.

[19] MATLAB, *version 7.10.0 (R2010a)*. The MathWorks Inc., 2010.

[20] N. Kimber and K. Scrimshaw, "Hydrodynamic testing of a 3/4 scale autosub model," *Proceedings of Oceanology International '94*, vol. 4, 1994.

[21] S. McPhail, "Autosub6000: A deep diving long range AUV," *Journal of Bionic Engineering*, vol. 6, no. 1, pp. 55 – 62, 2009.

[22] A. Phillips, L. Steenson, C. Harris, E. Rogers, S. Turnock, and M. Furlong, "Delphin2: An over actuated autonomous underwater vehicle for manoeuvring research," *The Transactions of the Royal Institution of Naval Architects, Part A - International Journal of Maritime Engineering*, 2013.

[23] D. Hudson, "User manual for program suite THARBM, three-dimensional analysis of rigid body motions," *School of Engineering Sciences, Ship Science, University of Southampton*, 2000.

[24] N. Townsend and R. Shenoi, "Modelling and analysis of a single gimbal gyroscopic energy harvester," *Nonlinear Dynamics*, vol. 72(1), pp. 285–300, 2013.

[25] K. Nandakumar, M. Wiercigroch, and A. Chatterjee, "Optimum energy extraction from rotational motion in a parametrically excited pendulum," *Mechanics Research Communications*, vol. 43, pp. 7–14, 2012.

[26] N. Townsend and R. Shenoi, "A gyroscopic wave energy recovery system for marine vessels," *IEEE Journal of Oceanic Engineering*, vol. 37(2), pp. 271–280, 2012.

[27] A. Phillips, M. Haroutunian, S. Man, A. Murphy, S. Boyd, J. Blake, and G. Griffiths, "Nature in engineering for monitoring the oceans: Comparison of the energetic costs of marine animals and AUVs," in *Further Advances in Unmanned Marine Vehicles*, R. Sutton and G. Roberts, Eds. Piscataway, New Jersey, USA: Institution of Engineering and Technology (IET), 2012.